Two-step modeling method for inverted pendulum considering Coulomb friction based on Lagrange equation and its model predictive control

Jianwei Wu, Beibei Sun*, Rui Huang and Zhao Peng

School of Mechanical Engineering, Southeast University, Nanjing, 211189, China
* (e-mail: bbsun@seu.edu.cn)

Abstract: To overcome the shortcomings associated with modeling difficulty from Coulomb friction and low accuracy from traditional methods, this paper proposes a two-step modeling method based on Lagrange equation for the inverted pendulum. After establishing the high nonlinear dynamic model, the model predictive control (MPC) is adopted for the inverted pendulum control and the satisfactory results are obtained. Furthermore, those studies—the comparisons of simulation and experiment from literature, the statistics of averaged computation time, the responses of no Coulomb friction, the responses of having constraints of maximum control force, and the influences of MPC parameters—are respectively carried out. Compared with experimental results from the literature, simulation results are effective and reliable, which further explain the fluctuation phenomenon caused by Coulomb friction after entering the stable state and thereby illustrate the higher accuracy of the model proposed in this paper. Moreover, simulation results demonstrate that MPC has obvious advantages of dealing with highly nonlinear system with constraints and hence has a high value of practical application, and also reveal that the control and prediction horizon risen properly can improve the response performance.

Keywords: Inverted pendulum, two-step modeling method, nonlinear model, Coulomb friction, MPC.

1. INTRODUCTION

Inverted pendulum, a typical multivariable, under-actuated, nonlinear, and strongly coupled unstable system, is one of the best model used for evaluating the performance of modern control methods. A high accuracy model applied for the control simulation is extremely important whether it can be used for real-time control for a physical model. To establish the model as accurately as possible, it is necessary to consider the nonlinear damping resulted from the friction or the parameter uncertainties caused by the manufacturing and assembly. Accordingly, a large number of studies have been carried out in order to improve the modeling accuracy of inverted pendulum, even applying the identification model to overcome the uncertainty encountered in modeling (Coxe, 2019; Hazem et al., 2020; Jadlovska et al., 2013; Muhammad et al., 2013; Shalaby et al., 2019; Tian et al., 2019).

Currently, there are mainly four methods used for dynamic modeling: Newton–Euler, Lagrange, Kane, and variational method (Balafoutis, 1994; Liu, 2016; Sandino et al., 2013). Among these methods, Lagrange equation of second kind uses the independent generalized coordinates to express the energy and work of the dynamic system, and then based on pure mathematical method obtains the differential equations whose number is equal to degrees of freedom. Due to the unified compact form, it has significant advantage when we manually deduce equations with a small number of degrees of freedom, which becomes the most popular modeling method for inverted pendulum.

When Lagrange equation of second kind is adopted for modeling of inverted pendulum, it is necessary to calculate the generalized force from friction by work involving in integral operation. Unfortunately, the work produced by Coulomb friction will cause great difficulties for the derivation of equation. Maybe "it is for this reason" that many researchers neglect the Coulomb friction and only consider the linear damping in modeling of inverted pendulum, and some even neglect damping (Andrzejewski et al., 2019; Chandra et al., 2019; Cruz et al., 2016; Hassanzadeh et al., 2011; Jadlovska et al., 2013; Shahab et al., 2017). Obviously, these modeling methods handling damping are inaccurate, and difficult to explain special phenomena (say the stable fluctuation phenomenon shown in this work) encountered in the experiment. Sometimes it can lead to a control failure in physical control owing to excessive error between the simulation and real models.

Therefore, to overcome the issue in modeling considering Coulomb friction, a two-step modeling method based on Lagrange equation of second kind is presented. At first, the dynamic equation of the inverted pendulum is established by using Lagrange equation of second kind without considering the damping, which obtains the dynamic equilibrium form with respect to force and moment similar to D' Alembert principle. Then, the Coulomb friction, viscous friction, and friction moment are directly added into the established equations without damping. It is noted that the plus or minus sign of the added force and moment depends on its direction with respect to the coordinate axes. In fact, the coordinate axes are reasonably defined to avoid these sign problems while modeling in this paper. After this operation, the high nonlinear dynamic equations of inverted pendulum are

obtained considering Coulomb friction, viscous friction, and friction moment.

After establishing the high nonlinear dynamic equations of inverted pendulum, the next crucial step is to select an appropriate control method for realizing the expected goals of inverted pendulum. In recent years, model predictive control (MPC) has achieved a great success in the application of industrial process control, widely employed for controlling linear or non-linear systems (Ji et al., 2017; Kayacan et al., 2018; Mayne, 2014; Xi et al., 2013; Yao et al., 2019). With the development of the intelligent driving technology, MPC due to its strong ability of dealing with constraints has been successfully applied in the fields of autonomous vehicles, unmanned aerial vehicles, and autonomous underwater vehicles (D Amato et al., 2020; Hu et al., 2020; Huang et al., 2019; Tan et al., 2019; Wang et al., 2020; Yao et al., 2018). As it turned out, the control method with input and output constraints, which is especially suitable for the practical problems encountered in engineering, has bright prospects.

MPC divided into linear model predictive control and nonlinear model predictive control (NMPC), and the abbreviation MPC generally denotes linear model control. In this paper, the linear model predictive control is adopted for inverted pendulum control, mainly based on the following three reasons.

First, NMPC is suitable for the dynamic model expressed by an analytic expression, otherwise the identification model is necessary to adopt, which increases the difficulty and uncertainty of modeling. Due to the introduction of Coulomb friction, the nonlinear dynamic model of inverted pendulum cannot be represented by a unified analytical expression, so it is not quite suitable for NMPC without identification model.

Second, when NMPC performs receding horizon optimization, its optimization model is not convex, and the efficiency and result of solution cannot be guaranteed for real-time control. For this reason, nonlinear model predictive control, currently, mostly stays in the stage of simulation research, and hence there are few practical applications. For the purpose of real-time control, linear model predictive control is also a better choice.

Third, a large amount of literature illustrates that linear model predictive control has a certain ability to deal with nonlinear system. Hence, one of the purposes of our research is to verify the conclusion by using the inverted pendulum model with the nonlinearity in this paper, hoping that MPC method can be popularize in more applications by the classical inverted pendulum model.

Although MPC has great advantages, especially in the aspect to deal with constraints, there are few studies on the computation time and influence of MPC parameters on response characteristics in the existing literature. Therefore, after establishing a highly nonlinear dynamic model for the inverted pendulum and verifying the simulation result by comparing with experimental results, we not only demonstrate its ability to handle the constraints, but also further analyze the computation time and influence of MPC parameters.

The rest of this paper is organized as follows. In Section 2, a highly nonlinear dynamic model for the inverted pendulum considering Coulomb friction, viscous friction, and friction moment is established based on the two-step modeling method proposed in this paper. In Section 3, MPC design process is introduced in detail. In Section 4, control simulations of inverted pendulum using MPC are implemented based on MATLAB programing, thereby obtaining simulation results. Furthermore, we compare the simulation with experimental results shown in literature (Shahab et al., 2017), make statistics of the averaged computation time under different MPC parameters, and respectively study the influences on response characteristics under the following three conditions: without Coulomb friction, with the constraints of maximum control force due to the physical limitations, and with different MPC parameters. Finally, conclusions are drawn in Section 5.

2. INVERTED PENDULUM MODEL

The single inverted pendulum model is shown in Fig. 1 where m and l respectively are the mass and length of the pendulum, M is the mass of the cart, u is the control input force, and g is the acceleration of gravity, the origin of the coordinate system is the rotation center of the pendulum and cart, the x-axis is vertically upward, the y-axis is horizontally leftward, and J is the pendulum moment of inertia of z-axis relative to the center of mass. The coordinate axis is given in Fig. 1, which can ensure that pendulum angle θ is angular deviation with its vertical inverted position and is positive value along with anti-clockwise direction.
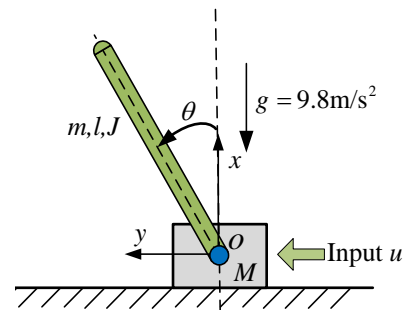
Fig. 1. Single inverted pendulum model.

2.1 Dynamical equation without damping

By using the Lagrange equations of second kind, the dynamical equation of single inverted pendulum model without damping can be obtained as

$$(M+m)\ddot{y}+m\ddot{\theta}L\cos(\theta)-m\dot{\theta}^2L\sin(\theta)=u \qquad (1)$$

$$mL\cos(\theta)\ddot{y}+J\ddot{\theta}+mL^2\ddot{\theta}-mL\dot{y}\dot{\theta}\sin(\theta)=mgL\sin(\theta) \qquad (2)$$

where $L=l/2$. After considering $J=mL^2/3$, Equations (1) and (2) can be concisely rewritten as

$$(M+m)\ddot{y}+m\ddot{\theta}L\cos(\theta)-m\dot{\theta}^2L\sin(\theta)=u \qquad (3)$$

$$\cos(\theta)\ddot{y}+\frac{4L}{3}\ddot{\theta}-\dot{y}\dot{\theta}\sin(\theta)=g\sin(\theta). \qquad (4)$$

2.2 Dynamical equation with damping using two-step modeling method

In fact, there are frictions between the cart and guideway and frictional resisting moment between the pendulum and cart, that is, the dynamical model of single inverted pendulum in practice exists damping. Here, it is assumed that the friction between the cart and the guideway is a combination of Coulomb and viscous friction, and the frictional resisting moment at the hinge joint is a linear damping (i.e. the linear relationship between frictional resisting moment and angular velocity of pendulum). When using the Lagrange equations of second kind deduces the dynamical equation with damping, it is necessary to calculate the generalized force from friction by work involving in integral operation. However, there exits work only when cart is moving due to Coulomb friction, which causes great difficulties for the derivation of equation.

By observing Equations (1) and (2) carefully, it can be seen that both sides of the equations are forces or moments. Actually, they are dynamic equilibrium form which can be obtained by D'Alembert principle. Accordingly, we only need to add damping force terms caused by the friction force and frictional resisting moment into Equations (1) and (2), and obtain the dynamical equations with damping. It is noted that plus or minus sign of the added force and moment depends on its direction with respect to the coordinate axes.

By taking the pendulum as the research object and according to the theorem of momentum, its dynamic equation on the *x*-axis can be expressed as

$$\frac{d}{dt}\left(-mL\dot{\theta}\sin\left(\theta\right)\right) = F_x - mg \tag{5}$$

where F_x denotes the force on *x*-axis from cart.

By applying the Newton's second law, the normal reaction force of cart can be obtained as

$$F_N = \left(M+m\right)g - mL\left(\dot{\theta}^2\cos\left(\theta\right) + \ddot{\theta}\sin\left(\theta\right)\right). \tag{6}$$

The friction force between cart and guideway can be expressed as

$$f = \mu\left(\left(M+m\right)g - mL\left(\dot{\theta}^2\cos\left(\theta\right) + \ddot{\theta}\sin\left(\theta\right)\right)\right) \tag{7}$$

where μ is coefficient of sliding friction.

Consider that the frictional resisting moment at the hinge joint is a linear damping; after adding damping force and moment into Equations (1) and (2), the dynamical equations can be written

$$\left(M+m\right)\ddot{y} + m\ddot{\theta}L\cos\left(\theta\right) = u +$$
$$\mu\left(-\left(M+m\right)g + mL\ddot{\theta}\sin\left(\theta\right) + mL\dot{\theta}^2\cos\left(\theta\right)\right)f_c\left(\dot{y}, v_c, v_0\right) -$$
$$c_M\dot{y}f_v\left(\dot{y}, v_c\right) + m\dot{\theta}^2L\sin\left(\theta\right)$$
$$\tag{8}$$

$$\cos\left(\theta\right)\ddot{y} + \frac{4L}{3}\ddot{\theta} = g\sin\left(\theta\right) + \dot{y}\dot{\theta}\sin\left(\theta\right) - \frac{c_m\dot{\theta}}{mL} \tag{9}$$

where c_M is the viscous damping coefficient between the cart and guideway, c_m is the damping coefficient from the frictional resisting moment at the hinge joint, $f_c(\bullet)$ denotes the Coulomb coefficient function whose curve is defined in Fig. 2, and $f_v(\bullet)$ denotes the viscous coefficient function whose curve is defined in Fig. 3. Here, it can be assumed that there exist v_0 and v_c which respectively denote the initial velocity (caused by Coulomb friction) that is going to work and the critical velocity that is going to move completely, as shown Figs. 2 and 3. For the purpose to control inverted pendulum, as a matter of fact, the cart must have certain velocity. In other words, Coulomb friction definitely exits, but viscous friction exits only when the cart velocity is greater than critical velocity v_c or less than critical velocity $-v_c$. In addition, the introduction of v_0 is mainly to avoid the ill-condition of numerical solution.
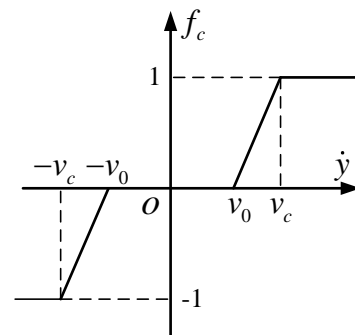
Fig. 2. Coulomb coefficient curve.
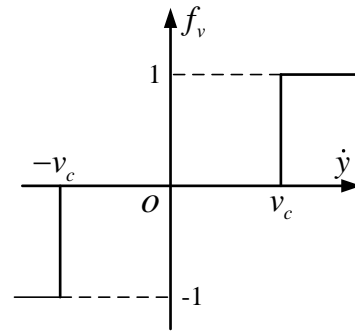
Fig. 3. Viscous coefficient curve.

Equation (8) is rearranged and simplified as

$$\left(M+m\right)\ddot{y} + m\ddot{\theta}L\left(\cos\left(\theta\right) - \mu\sin\left(\theta\right)f_c\left(\dot{y}, v_c, v_0\right)\right) =$$
$$u - \mu\left(M+m\right)gf_c\left(\dot{y}, v_c, v_0\right) -$$
$$c_M\dot{y}f_v\left(\dot{y}, v_c\right) + m\dot{\theta}^2L\left(\sin\left(\theta\right) + \mu\cos\left(\theta\right)f_c\left(\dot{y}, v_c, v_0\right)\right).$$
$$\tag{10}$$

It can be found that Equations (9) and (10) are highly nonlinear equations only by means of the numerical method to solve. In general, μ is 0.15 for dry friction or 0.05-0.1 for lubricated Friction. Because μ is very small, coefficient matrix with respect to $\ddot{y}$ and $\ddot{\theta}$ in Equations (9) and (10) is invertible. For the convenience to solve using numerical method, therefore, the dynamical equation of single inverted pendulum with damping can be expressed as

$$\begin{bmatrix} \ddot{y} \\ \ddot{\theta} \end{bmatrix} = \dfrac{\begin{bmatrix} \dfrac{4L}{3}\left\{ u - c_M \dot{y} f_v(\dot{y}, v_c) - \mu(M+m)g f_c(\dot{y}, v_c, v_0) + m\dot{\theta}^2 L\left(\sin(\theta) + \mu\cos(\theta) f_c(\dot{y}, v_c, v_0)\right) \right\} - \\ mL\left(\cos(\theta) - \mu\sin(\theta) f_c(\dot{y}, v_c, v_0)\right)\left\{ g\sin(\theta) + \dot{y}\dot{\theta}\sin(\theta) - \dfrac{c_m \dot{\theta}}{mL} \right\} \\ -\cos(\theta)\left\{ u - c_M \dot{y} f_v(\dot{y}, v_c) - \mu(M+m)g f_c(\dot{y}, v_c, v_0) + m\dot{\theta}^2 L\left(\sin(\theta) + \mu\cos(\theta) f_c(\dot{y}, v_c, v_0)\right) \right\} + \\ (M+m)\left\{ g\sin(\theta) + \dot{y}\dot{\theta}\sin(\theta) - \dfrac{c_m \dot{\theta}}{mL} \right\} \end{bmatrix}}{\dfrac{4L}{3}(M+m) - mL\cos(\theta)\left(\cos(\theta) - \mu\sin(\theta)\cdot f_c(\dot{y}, v_c, v_0)\right)}. \quad (11)$$

When the input u is given, system responses can be obtained by numerical solution according to Equation (11). After establishing the dynamical equation, we can design controller to realize the control goals that the pendulum turns towards the inverted vertical position (i.e. θ=0) and that the cart moves to the original position (i.e. y=0) under certain disturbance.

3. DESIGN OF MPC

3.1 Linearized dynamical equation and its augmented state-space model

Suppose that the pendulum angle is very small, neglect second order small quantity, and let $X = \begin{bmatrix} y & \dot{y} & \theta & \dot{\theta} \end{bmatrix}^T$, and then Equations (3) and (4) can be written the state equation form considering y and θ as outputs

$$\dot{X} = AX + Bu \quad (12)$$

$$Y = CX \quad (13)$$

where

$$A = \begin{bmatrix} 0 & 1 & 0 & 0 \\ 0 & 0 & -\dfrac{3mg}{(4M+m)} & 0 \\ 0 & 0 & 0 & 1 \\ 0 & 0 & \dfrac{3(M+m)g}{(4M+m)L} & 0 \end{bmatrix}, \quad B = \begin{bmatrix} 0 \\ \dfrac{4}{(4M+m)} \\ 0 \\ -\dfrac{3}{(4M+m)L} \end{bmatrix},$$

$$C = \begin{bmatrix} 1 & 0 & 0 & 0 \\ 0 & 0 & 1 & 0 \end{bmatrix}. \quad (14)$$

In general, the system to be controlled is modeled by discrete state-space model in the MPC literature (Liuping, 2009; Ridong et al., 2019). Therefore, Equations (12) and (13) are transformed into the discrete state-space model as

$$X_d(k+1) = A_d X_d(k) + B_d u(k) \quad (15)$$

where A_d and B_d are the state and control matrices for the discrete state-space equation, respectively, which can be accurately calculated as

$$A_d = e^{A\Delta T} \quad (16)$$

$$B_d = \int_0^{\Delta T} e^{At} dt \cdot B \quad (17)$$

where ΔT is the sampling interval for the discrete state-space model.

The pendulum angle and cart displacement are defined as outputs variables as

$$Y_d(k) = C_d X_d(k) \quad (18)$$

where $C_d = C$.

For convenience to control using MPC, the incremental forms of the control, state, and output variables are defined as

$$\Delta X_d(k+1) = A_d \Delta X_d(k) + B_d \Delta u(k) \quad (19)$$

$$Y_d(k+1) - Y_d(k) = C_d A_d \Delta X_d(k) + C_d B_d \Delta u(k) \quad (20)$$

where $\Delta X_d(k+1) = X_d(k+1) - X_d(k)$,
$\Delta X_d(k) = X_d(k) - X_d(k-1)$, $\Delta u(k) = u(k) - u(k-1)$.

Next, define a new state variable

$$X_a(k) = \begin{bmatrix} \Delta X_d(k) \\ Y(k) \end{bmatrix}_{6\times 1}. \quad (21)$$

By Equations (19)–(21), the following state-space model can be obtained as

$$X_a(k+1) = (A_a)_{6\times 6} X_a(k) + (B_a)_{6\times 1} \Delta u(k) \quad (22)$$

$$Y_a(k) = (C_a)_{2\times 6} X_a(k) \quad (23)$$

where the triplet (A_a, B_a, C_a) are called the augmented model, which can be described as follows:

$$A_a = \begin{bmatrix} A_d & O_a^T \\ C_d A_d & I_a \end{bmatrix}, B_a = \begin{bmatrix} B_d \\ C_d B_d \end{bmatrix}, C_a = \begin{bmatrix} O_a & I_a \end{bmatrix},$$

$$O_a = \begin{bmatrix} 0 & 0 & 0 & 0 \\ 0 & 0 & 0 & 0 \end{bmatrix}, I_a = \begin{bmatrix} 1 & 0 \\ 0 & 1 \end{bmatrix}. \quad (24)$$

3.2 Prediction of state and output variables

According to Equation (21), we have

$$X_m(k) = X_a(k) = $$
$$\begin{bmatrix} \Delta y(k) & \Delta \dot{y}(k) & \Delta \varphi(k) & \Delta \dot{\varphi}(k) & y(k) & \varphi(k) \end{bmatrix}^T. \quad (25)$$

An important step for MPC is to predict the future behavior according to linear or nonlinear dynamic mode, so it is

necessary to define the prediction horizon N_p and control horizon N_c in advance. With given information $X_a(k)$ calculated by simulating or measured by sensor, the future state variables can be predicted for N_p step ahead, as follows:

$$X_a(k+1), X_a(k+2), \cdots, X_a(k+m), \cdots, X_a(k+N_p) \qquad (26)$$

where $X_a(k+m)$ is the predicted state variable at $k+m$ with given current plant information $X_a(k)$.

Since the control horizon is N_c, we denoted by ΔU_m the sequence of future input increments as

$$\Delta U_m = \left[\Delta u(k), \cdots, \Delta u(k+m), \cdots, \Delta u(k+N_c-1) \right]^T. \qquad (27)$$

It should be noted that input increment in the control horizon is variable while remains constant outside the control horizon.

Then, we define

$$Y_m(k) = \left[Y_a(k)^T, Y_a(k+1)^T, \cdots, Y_a(k+N_p)^T \right]^T. \qquad (28)$$

By Equations (22), (23) and (25)–(28), the compact matrix form can be obtained as (Liuping, 2009; Ridong et al., 2019)

$$Y_m(k) = F_m X_m(k) + G_m \Delta U_m \qquad (29)$$

$$F_m = \left[(C_a A_a)^T, \cdots, (C_a A_a^{N_c})^T, \cdots, (C_a A_a^{N_p})^T \right]^T_{2N_p \times 6} \qquad (30)$$

$$G_m = \begin{bmatrix} C_a B_a & 0 & \cdots & 0 \\ C_a A_a B_a & C_a B_a & \cdots & 0 \\ \vdots & \vdots & \cdots & \vdots \\ C_a A_a^{N_c-1} B_a & C_a A_a^{N_c-2} B_a & \cdots & C_a B_a \\ \vdots & \vdots & \ddots & \vdots \\ C_a A_a^{N_p-1} B_a & C_a A_a^{N_p-2} B_a & \cdots & C_a A_a^{N_p-N_c} B_a \end{bmatrix}_{2N_p \times N_c} \qquad (31)$$

3.3 Cost function

Considering control goals that the pendulum turns towards the inverted vertical position (i.e. $\theta=0$) and that the cart moves to the original position (i.e. $y=0$) under certain disturbance, we have the reference outputs in the prediction horizon as follows

$$R(k) = \left[0, 0, \cdots, 0, 0 \right]^T_{2N_p \times 1}. \qquad (32)$$

The predictive outputs can be expressed as

$$Y_m(k) = \left[y(k+1), \theta(k+1) \cdots, y(k+N_p), \theta(k+N_p) \right]^T_{2N_p \times 1}. \qquad (33)$$

Define ω_1, ω_2 and ω_3 which express the weights of the cart displacement, pendulum angle and input increment, respectively. Then the cost function is given by

$$J_E = \left[R(k) - Y_m(k) \right]^T Q \left[R(k) - Y_m(k) \right] + \Delta U_m^T R \Delta U_m \qquad (34)$$
$$= Y_m(k)^T Q Y_m(k) + \Delta U_m^T R \Delta U_m$$

where

$$Q = \begin{bmatrix} \begin{bmatrix} \omega_1 & \\ & \omega_2 \end{bmatrix} & & & \\ & \ddots & & \\ & & \begin{bmatrix} \omega_1 & \\ & \omega_2 \end{bmatrix} \end{bmatrix}_{2N_p \times 2N_p}, R = \omega_3 I_{N_c \times N_c}. \qquad (35)$$

By according to Equation (29) and neglecting the unrelated terms with ΔU_m, J_E can be rewritten as

$$J_E = \frac{1}{2} \Delta U_m^T R_m \Delta U_m + \Delta U_m^T E_m \qquad (36)$$

where

$$R_m = 2 \left(G_m^T Q G_m + R \right), \ E_m = 2 G_m^T Q F_m X_m(k). \qquad (37)$$

3.4 Constraints for MPC

The obvious advantage of MPC is able to deal with constraints with input and output, which can satisfy actual requirements. There are three major types of constraints as follows:

$$-C_1 u_{max} \le C_1 u(k-1) + C_2 \Delta U_m \le C_1 u_{max} \qquad (38)$$

$$-C_1 \Delta u_{max} \le \Delta U_m \le C_1 \Delta u_{max} \qquad (39)$$

$$C_3 \begin{bmatrix} -y_{max} \\ -\theta_{max} \end{bmatrix} \le F_m X_m(k) + G_m \Delta U_m \le C_3 \begin{bmatrix} y_{max} \\ \theta_{max} \end{bmatrix} \qquad (40)$$

where u_{max} and Δu_{max} respectively denote the allowable maximums of the input and input rate determined by the engineering realization, and y_{max} and θ_{max} respectively denote the allowable maximums of the cart displacement and pendulum angle. In Equations (38)–(40), there are

$$C_1 = \begin{bmatrix} 1 \\ 1 \\ \vdots \\ 1 \end{bmatrix}_{N_c \times 1}, C_2 = \begin{bmatrix} 1 & 0 & 0 & 0 \\ 1 & 1 & 0 & 0 \\ \vdots & \vdots & \ddots & \vdots \\ 1 & 1 & \cdots & 1 \end{bmatrix}_{N_c \times N_c}, C_3 = \begin{bmatrix} 1 & 0 \\ 0 & 1 \\ \vdots & \vdots \\ 1 & 0 \\ 0 & 1 \end{bmatrix}_{2N_p \times 2}. \qquad (41)$$

These constraints can be written as the following linear matrix inequality form

$$M_m \Delta U \le N_m \qquad (42)$$

where

$$M_m = \begin{bmatrix} \begin{bmatrix} -C_2 \\ C_2 \end{bmatrix} \\ \begin{bmatrix} -I_{N_c \times N_c} \\ I_{N_c \times N_c} \end{bmatrix} \\ \begin{bmatrix} -G_m \\ G_m \end{bmatrix} \end{bmatrix}_{(4N_c + 4N_p) \times N_c}, $$

$$N_m = \begin{bmatrix} \begin{bmatrix} C_1 u_{max} + C_1 u(k-1) \\ C_1 u_{max} - C_1 u(k-1) \end{bmatrix} \\ \begin{bmatrix} \Delta u_{max} C_1 \\ \Delta u_{max} C_1 \end{bmatrix} \\ -C_3 \begin{bmatrix} -x_{max} \\ -\theta_{max} \end{bmatrix} + F_m X_m(k) \\ C_3 \begin{bmatrix} x_{max} \\ \theta_{max} \end{bmatrix} - F_m X_m(k) \end{bmatrix}_{(4N_c + 4N_p) \times 1} \quad (43)$$

3.5 Receding horizon optimization for MPC

Generally, the input and input rate constraints are called hard constraints (Equations (38–39)), while the output constraints are called soft constraints (Equation (40)). Because of the limitation of physical conditions, the hard constraints must be satisfied, while the soft constraints are determined largely by the hard constraints, so they can be violated owing to the conflict between the hard and soft constraints.

According to Equations (36) and (42), it is observed that the problem, which minimizes cost function with linear inequality constraints, is a quadratic convex optimization with respect to ΔU_m. Hence, ΔU_m has a global optimum solution, when there is no conflict between the hard and soft constraints. But if there is a conflict between them, the global optimal solution will be obtained by satisfying the hard constraints and neglecting the soft constraints.

By Equations (36) and (42), the existing quadratic programming function with linear matrix inequality constraints can be directly used for solution, but it is necessary to take a certain mechanism for dealing with the soft and hard constraints. After the optimal incremental sequence of control input is obtained by optimization, the first control increment is selected to calculate the response to impose on the nonlinear inverted pendulum model. Then the prediction and optimization is implemented according to the current response. The process (i.e. receding horizon) of the prediction, optimization and selection, will be finished up to the end time.

As can be seen above, an online optimization solution is needed in every time step, which has a great influence on real-time control. It is the drawback that exists in the MPC. With the continuous improvement of the computer hardware and algorithm, fortunately, the problem has been basically solved for linear model predictive control.

4. SIMULATION AND DISCUSSIONS

To investigate the performance and parameter influence of MPC, numerical simulations will be implemented based on MATLAB programing, and the numerical simulation process is shown in Fig. 4.
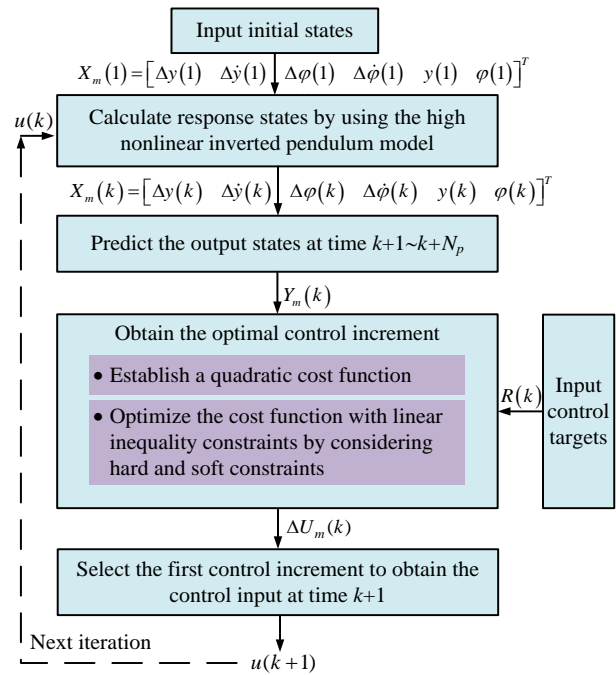
Fig. 4. Simulation process for MPC.

4.1 Simulation parameters and computer configurations

For comparison with experimental results, the simulation parameters of single inverted pendulum from literature (Shahab et al., 2017) are shown in Table 1.

Table 1. Simulation parameters of single inverted pendulum.

Symbol	Value	Unit
M	1.02	kg
m	0.49	kg
L	0.2	m
μ	0.05	–
c_M	21.06	N·m·s/rad
c_m	0.009	N·s/m
v_0	0.001	mm/s
v_c	0.1	mm/s
g	9.8	m/s^2

To study the computation time in section 4.3, we give the computer configurations for simulation as follows.

Operating system: windows 7 with 64 bit

CPU: Intel(R) Core(TM) i7-3667U

RAM: 8GB with 1333MHz

MATLAB versions: MATLAB 2012a

4.2 MPC Simulation results and discussions

In this section, firstly, we give the MPC simulation results for the inverted pendulum based on the process shown in Fig. 4, and compare them with the experimental results from the

literature (Shahab et al., 2017). Then, the simulation results for the inverted pendulum with and without damping are contrasted. Finally, we obtain the MPC simulation for the inverted pendulum under the condition with restrict maximum control force results.

Because MPC needs to be optimized at every time step, in order to ensure the real-time control requirements, the sampling time generally is not too small. In addition, with the increase of prediction and control horizon, the optimization time will dramatically increase. Therefore, based on trial-and-error process and experience, the parameters of MPC controller are given, as shown in Table 2.

Table 2. Parameters of MPC controller.

Symbol	Value	Unit
N_p	15	–
N_c	8	–
ΔT	0.05	s
T	10	s
u_{max}	500	N
Δu_{max}	500	N/s
y_{max}	1	m
θ_{max}	1.2	rad
ω_1	1	–
ω_2	5	–
ω_3	0.001	–

After initial state is given as $X_0 = \begin{bmatrix} 0 & 0 & 0.8 & 0 \end{bmatrix}^T$, the simulation results expressed by black curves can be obtained by performing the developed program based on MATLAB, as shown in Figs. 5–7. To clearly observe the fluctuation of curves after the system remains stable, the enlarged views at 6–10 s are respectively shown in Figs. 5–7.

It can be seen from the Figs. 5–7 that, under the given initial state and MPC controller parameters, the inverted pendulum tends to be stable after 2 s, which illustrates that MPC achieved the expected control goals that both the cart displacement and the pendulum angle are gradually close to 0. In addition, it is carefully observed that black curves in Figs. 5–7 slightly fluctuate along with their respective control goals after the settling time. When meticulously observed the experimental results of the pendulum angle in literature (Shahab et al., 2017), it also slightly fluctuates along with the target, which illustrates that the results in this paper are consistent with experiments well. Similarly, the fluctuation phenomenon also exists in experiment results (Guo et al., 2014; Haddad et al., 2018; Maity et al., 2019; Tang et al., 2020). However, it should be noted the unit and range of y-axis in Fig. 15 from the literature (Shahab et al., 2017), because the curve fluctuation is seemingly not obvious. In fact, the simulation results in this paper are considerably consistent with experimental results if experimental curves maintain same unit and range of y-axis with Figs. 5–7.
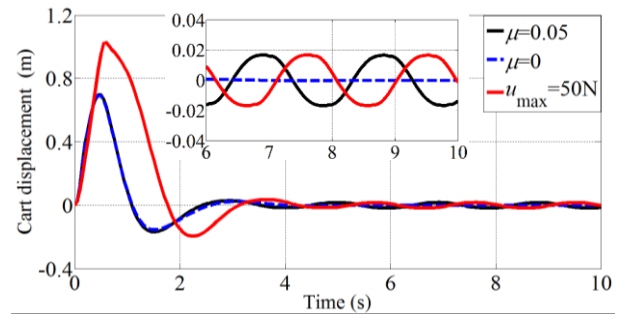
Fig. 5. Response of cart displacement.
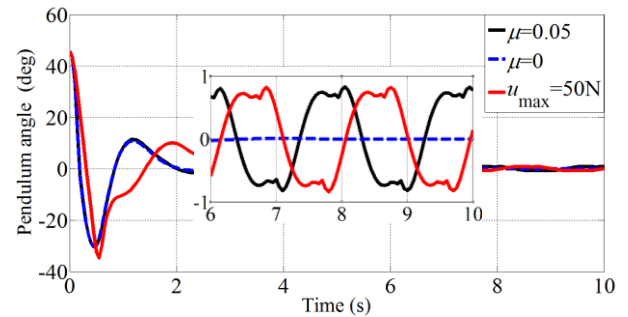
Fig. 6. Response of pendulum angle.
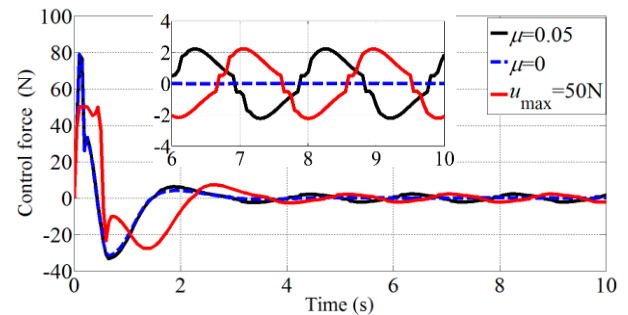
Fig. 7. Response of control force.

Theoretically, the stable fluctuation is also easily explained. On the one hand, in order to control pendulum angle, the cart must have a certain velocity, so the control force in Fig. 7 at this time must be enough to overcome the Coulomb friction. On the other hand, in order to control displacement of cart with a certain velocity, a reverse control force is applied to the cart, leading to that the pendulum angle is deviated from 0. Subsequently, the pendulum angle will be controlled again, and so forth, generating the black curves with fluctuation as depicted Figs. 5–7.

From above the theoretical analysis, it can be known that if no Coulomb friction (i.e. $\mu = 0$), there is not a stable fluctuation after the settling time. The simulation results without Coulomb friction is shown in blue curves in Figs. 5–7, verifying the correctness of theoretical analysis.

MPC have ability to deal with constraints. To further demonstrate its advantage, we assume that the maximum control force that the system can provide is 50 N (i.e. $u_{max} = 50N$) due to physical limits. Then, the simulation results expressed by red curves can be obtained, as shown in Figs. 5–7. Note that there is Coulomb friction ($\mu = 0.05$) in this

simulation results of red curves, and it is just that the constraint of maximum control force is different from black curves, as shown in Figs. 5–7. It can be seen from the red curves shown in Figs. 5–7 that, the control force applied to the cart will not exceed 50 N, which also achieves the expected control effect according to the response results of cart displacement and pendulum angle. However, under the limit of maximum control force being 50 N, the amplitudes of the cart displacement and pendulum angle increase to a certain extent, and the settling time is delayed slightly.

In short, compared with the experimental results from literature (Shahab et al., 2017), simulation results using the supposition modeling method considering Coulomb friction is effective and more accurate for MPC in this paper. Next section will further study the influence of MPC parameters on response results.

4.3 Influence analysis of MPC parameters

The methods based on trial-and-error process and experience, however, cannot quickly be used to design MPC controller. Because of this drawback, the influence on simulation results from MPC parameters will be researched in this section.

Table 3 shows five combinations caused by the changes of the prediction horizon and control horizon, and the other parameters remain the same with Table 2. The last row in the Table 3 lists computation time that is statistical average performing 20 times same simulations in their respective parameter combinations. It is clear that with the increase of the prediction horizons and control horizons, the averaged computation time gradually increases. By comparing the simulation time (10 s) with averaged computation time shown in Table 3, obviously, computer configurations meet the requirement of the real-time control.

Table 3. Five combinations of controller parameters for MPC.

	1	2	3	4	5
N_p	15	15	15	10	20
N_c	2	5	8	5	5
Averaged computation time (s)	1.29	1.35	1.52	1.21	1.55

Figs. 8–10 show the simulation results of cart displacement, pendulum angle, and control force under different control horizons while prediction horizon remains unchanged. It can be seen that as the control horizon increases, setting time decreases, but the influences of these amplitudes are not apparent. Besides, with the increase of control horizon, the response curves become steeper, which improves the transient response to some degree.

Theoretically, it is easier to explain these simulation results as shown in Fig. 8–10. With the increase of control horizon, the amount used for control increases. To minimize the performance index (Equation (36)), it will make full use of the control sequence to make the system stable as soon as possible.
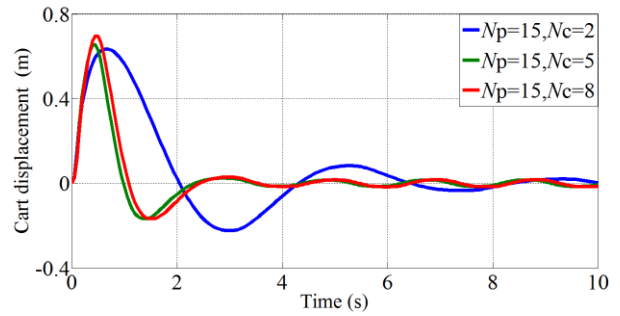
Fig. 8. Response of cart displacement under different control horizons.
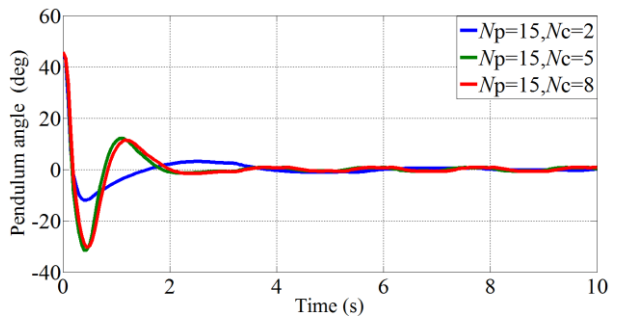
Fig. 9. Response of pendulum angle under different control horizons.
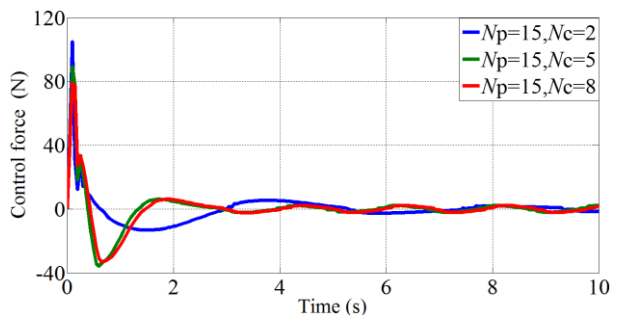
Fig. 10. Response of control force under different control horizons.

Figs. 11–13 show the simulation results of the cart displacement, pendulum angle, and control force under different prediction horizons while the control horizon N_c remains unchanged. With the rise of the prediction horizons, the responses in Figs. 11–13 have the similar characteristics with the counterparts in Figs. 8–10. Theoretically, it is also easier to explain these results shown in Fig. 11–13. With the increase of prediction horizon, the future information that can be obtained increases accordingly, and it will take full advantage of the control sequence to minimize the performance index during longer period of time, ensuring that the system enters the stable state more fast (that is, settling time will shorten).

In a word, the simulation results shown in Figs. 8–13 indicate that appropriately increasing the control horizon and prediction horizon can improve the response performance under the premises that the requirement of real-time control is satisfied and that the predictive model is accurate enough with real model.
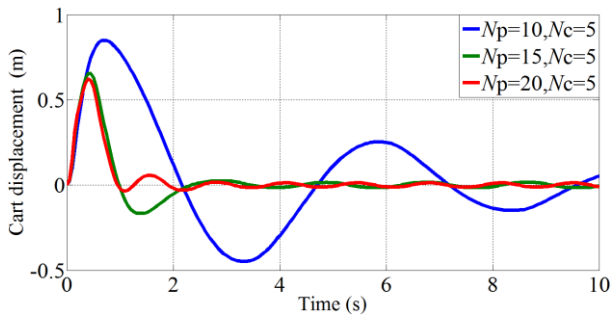
Fig. 11. Response of cart displacement under different prediction horizons.
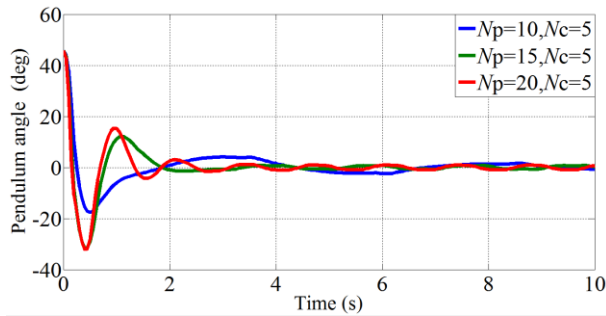
Fig. 12. Response of pendulum angle under different prediction horizons.
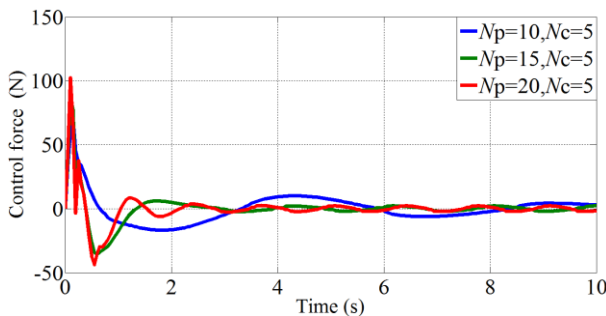
Fig. 13. Response of control force under different prediction horizons.

5. CONCLUSIONS

In this paper, a two-step modeling method of inverted pendulum based on Lagrange equation is proposed, improving the modeling accuracy by considering the Coulomb friction. Then, the MPC is adopted for the inverted pendulum control and the satisfactory results are obtained. Furthermore, we compare the simulation with experimental results shown in literature (Shahab et al., 2017), make statistics of the averaged computation time under different MPC parameters, and respectively study the influences on response characteristics under the following three conditions: without Coulomb friction, with the constraints of maximum control force due to the physical limitations, and with different MPC parameters. Through the above studies, the conclusions can be drawn as follows.

(1) The concept of two-step modeling method based on Lagrange equation for the inverted pendulum is simple and easy to understand. In addition, this method can be easily extended to the dynamic modeling of a multistage inverted pendulum.

(2) The simulation results using the highly nonlinear dynamic model that considers the Coulomb friction for inverted pendulum can better reflect the experimental results, illustrating that the model proposed in the paper have a higher accuracy than previous models and the simulation results are effective and reliable.

(3) Stable fluctuations of the simulation and experimental curves after the settling time are caused by Coulomb friction.

(4) Linear model predictive control can perform effectively control under the constraints, and also is able to deal with the certain nonlinear systems, which has significant advantages in practical application.

(5) The averaged computation time gradually increases with the increase of prediction and control horizons.

(6) Simulation results indicate that the control and prediction horizon risen properly can improve the response performance under the premises that the requirement of real-time control is satisfied and that the predictive model is accurate enough with real model.

REFERENCES

Andrzejewski, K., Czyzniewski, M., Zielonka, M., Langowski, R., Zubowicz, T. (2019) A Comprehensive Approach to Double Inverted Pendulum Modelling. *Archives of Control Sciences*, 29(3), 459-483.

Balafoutis, C.A. (1994) A Survey of Efficient Computational Methods for Manipulator Inverse Dynamics. *Journal of Intelligent & Robotic Systems*, 9(1-2), 45-71.

Chandra, J., Tamba, T.A., Sadiyoko, A. (2019) Energy-Based Modeling and Swing Up Control Synthesis of an Inverted Pendulum System. 2019 International Conference on Mechatronics, Robotics and Systems Engineering (MoRSE), pp. 265-269.

Coxe, A.M. (2019) Neural Control Model for an Inverted Double Pendulum. *Complex Systems*, 28(2), 239-249.

Cruz, D., Garcia, S., Bandala, M. (2016) Ann-Based Control of a Wheeled Inverted Pendulum System Using an Extended Dbd Learning Algorithm. *International Journal of Advanced Robotic Systems*, 13(3), 1-11.

D Amato, E., Mattei, M., Notaro, I. (2020) Distributed Reactive Model Predictive Control for Collision Avoidance of Unmanned Aerial Vehicles in Civil Airspace. *Journal of Intelligent & Robotic Systems*, 97(1), 185-203.

Guo, Z., Xu, J., Lee, T.H. (2014) Design and Implementation of a New Sliding Mode Controller On an Underactuated Wheeled Inverted Pendulum. *Journal of the Franklin Institute*, 351(4), 2261-2282.

Haddad, N.K., Chemori, A., Belghith, S. (2018) Robustness Enhancement of Ida-Pbc Controller in Stabilising the Inertia Wheel Inverted Pendulum: Theory and Real-

Time Experiments. *International Journal of Control: Estimation and Control of Multidimensional Systems*, 91(12), 2657-2672.

Hassanzadeh, I., Nejadfard, A., Zadi, M. (2011) A Multivariable Adaptive Control Approach for Stabilization of a Cart-Type Double Inverted Pendulum. *Mathematical Problems in Engineering* (doi: 10.1155/2011/970786), 970786:1-14.

Hazem, Z.B., Fotuhi, M.J., Bingül, Z. (2020) A Comparative Study of the Joint Neuro-Fuzzy Friction Models for a Triple Link Rotary Inverted Pendulum. *Ieee Access*, 8, 49066-49078.

Hu, J., Xiong, S., Zha, J., Fu, C. (2020) Lane Detection and Trajectory Tracking Control of Autonomous Vehicle Based On Model Predictive Control. *International Journal of Automotive Technology*, 21(2), 285-295.

Huang, Y., Wang, H., Khajepour, A., Ding, H., Yuan, K., Qin, Y. (2019) A Novel Local Motion Planning Framework for Autonomous Vehicles Based On Resistance Network and Model Predictive Control. *Ieee Transactions On Vehicular Technology*, 69(1), 55-66.

Jadlovska, S., Sarnovsky, J. (2013) Modelling of Classical and Rotary Inverted Pendulum Systems - A Generalized Approach. *Journal of Electrical Engineering-Elektrotechnicky Casopis*, 64(1), 12-19.

Ji, J., Khajepour, A., Melek, W.W., Huang, Y. (2017) Path Planning and Tracking for Vehicle Collision Avoidance Based On Model Predictive Control with Multiconstraints. *Ieee Transactions On Vehicular Technology*, 66(2), 952-964.

Kayacan, E., Saeys, W., Ramon, H., Belta, C., Peschel, J.M. (2018) Experimental Validation of Linear and Nonlinear Mpc On an Articulated Unmanned Ground Vehicle. *Ieee-Asme Transactions On Mechatronics*, 23(5), 2023-2030.

Liu, Y. (2016) *Advanced Dynamics*. Higher education press, Beijing, China.

Liuping, W. (2009) *Model Predictive Control System Design and Implementation Using Matlab®*. Springer, London.

Maity, S., Luecke, G.R. (2019) Stabilization and Optimization of Design Parameters for Control of Inverted Pendulum. *Journal of Dynamic Systems Measurement and Control-Transactions of the Asme*, 141(8).

Mayne, D.Q. (2014) Model Predictive Control: Recent Developments and Future Promise. *Automatica*, 50(12), 2967-2986.

Muhammad, M., Buyamin, S., Ahmad, M.N., Nawawi, S.W.

(2013) Takagi-Sugeno Fuzzy Modeling of a Two-Wheeled Inverted Pendulum Robot. *Journal of Intelligent & Fuzzy Systems*, 25(3), 535-546.

Ridong, Z., Anke, X., Furong, G. (2019) *Model Predictive Control*. Springer, Singapore.

Sandino, L.A., Bejar, M., Ollero, A. (2013) A Survey On Methods for Elaborated Modeling of the Mechanics of a Small-Size Helicopter. Analysis and Comparison. *Journal of Intelligent & Robotic Systems*, 72(2), 219-238.

Shahab, E., Nikoobin, A., Ghoddosian, A. (2017) Indirect-Based Approach for Optimal Svving Up and Stabilization of a Single Inverted Pendulum with Experimental Validation. *Control Engineering and Applied Informatics*, 19(4), 61-71.

Shalaby, R., El-Hossainy, M., Abo-Zalam, B. (2019) Fractional Order Modeling and Control for Under-Actuated Inverted Pendulum. *Communications in Nonlinear Science and Numerical Simulation*, 74, 97-121.

Tan, Y., Cai, G., Li, B., Teo, K.L., Wang, S. (2019) Stochastic Model Predictive Control for the Set Point Tracking of Unmanned Surface Vehicles. *Ieee Access*, 8, 579-588.

Tang, T.F., Chong, S.H., Pang, K.K. (2020) Stabilisation of a Rotary Inverted Pendulum System with Double-Pid and Lqr Control: Experimental Verification. *International Journal of Automation and Control*, 14(1), 18-33.

Tian, X., Peng, H., Zhou, F., Peng, X. (2019) Rbf-Arx Model-Based Fast Robust Mpc Approach to an Inverted Pendulum. *Isa Transactions*, 93, 255-267.

Wang, X., Yao, X., Zhang, L. (2020) Path Planning Under Constraints and Path Following Control of Autonomous Underwater Vehicle with Dynamical Uncertainties and Wave Disturbances. *Journal of Intelligent & Robotic Systems*, 99(3-4), 891-908.

Xi, Y., Li, D., Lin, S. (2013) Model Predictive Control Status and Challenges. *Acta Automatica Sinica*, 39(3), 222-236.

Yao, F., Yang, C., Liu, X., Zhang, M. (2018) Experimental Evaluation On Depth Control Using Improved Model Predictive Control for Autonomous Underwater Vehicle (Auvs). *Sensors*, 18(7), 2321:1-16.

Yao, Q., Tian, Y. (2019) A Model Predictive Controller with Longitudinal Speed Compensation for Autonomous Vehicle Path Tracking. *Applied Sciences-Basel*, 9(22), 1-17.